APPENDIX A: PRELIMINARY BOREHOLE TO SEA CLIFF CORRELATIONS, X-RAY DIFFRACTION AND SEM ANALYSIS OF SLIP PLANE, AND GRAIN SIZE STUDY OF SEDIMENTARY UNITS OF THE JOHNSON CREEK LANDSLIDE ON U.S. HIGHWAY 101, CENTRAL COAST OF OREGON, NORTH OF NEWPORT

by Alan R. Niem
Professor Emeritus of Geology
Oregon State University
Oregon Registered Geologist #G659

submitted to DOGAMI on April 9, 2003
revised June 25, 2003

EXECUTIVE SUMMARY AND RECOMMENDATIONS

Dr. Alan Niem was contracted by DOGAMI to provide information to DOGAMI, ODOT, and Landslide Technology on the geologic nature and controls of the Johnson Creek landslide on the central Oregon coast north of Newport (Figure A1). This preliminary report consists of (1) a detailed discussion of east-west lithologic correlation of boreholes LT-1, LT-2, and LT-3 to a sea cliff section at the toe of the landslide, (2) x-ray diffraction (XRD) study of the mineralogical and microscopic (e.g., scanning electron microscope [SEM]) causes of slope failure, and (3) statistical grain size and thin section analysis of the stratigraphic section with emphasis on the lower and middle Miocene Astoria Formation exposed in the sea cliff at the toe of the landslide to determine the potential of these strata to contribute to the modern littoral sand budget.

RESULTS

1. Borehole and Sea Cliff Correlation

The Pleistocene terrace deposit in the upper part of the three boreholes consists of densely packed, well-sorted, reddish yellow iron oxide-stained, friable, fine to medium sand, 11 to 20 ft thick, a local paleosol (in LT-1), and a rounded siltstone cobble at the base of the deposit (in LT-2) (Plate AI correlation diagram). Some sediment in the base of the terrace deposit is compositionally and texturally similar to the paleo-surge channel-fill quartzo-feldspathic-lithic (mainly Astoria mudstone clasts) terrace sand and gravel that overlie the angular unconformity on the Astoria Formation exposed a short distance east of the headscarp on the Boise Cascade logging road. Pleistocene terrace beach sands in the sea cliffs and headscarp consist of locally case-hardened, well-sorted, fine and some medium beach sand (mainly subrounded grains of quartz, feldspar, and lithics [volcanic]) and a fluvial sandy gravel channel fill with framework-supported, rounded, white gibbsite, quartz, and Columbia River Basalt pebbles. These gravel lenses are overlain by a gray paleosol with gley or E-horizon and a dark, organic-rich A horizon. The Pleistocene deposits and the Miocene Astoria Formation are locally overlain and partly covered by thin to thick, surficial, Holocene landslide toe colluvium composed of mostly poorly sorted angular clasts of Astoria Formation siltstone in a reworked Pleistocene terrace sand matrix (see middle sea cliff section on Plate AI). The maximum vertical displacement by landsliding of the angular unconformity between the Quaternary terrace deposit and the underlying lower and middle Miocene Astoria Formation is calculated to be 70 feet on a 1:1 scale cross section between its position just east of the headscarp through the three boreholes to its position in the sea cliffs at the toe of the landslide (Plate AI, cross section B).

Composite thickness of the Astoria Formation correlated in the three boreholes and exposed in the sea cliff is 140 ft. These 140 ft of strata include four stratigraphic sequences of shallow-marine (inner to middle shelf), fossil mollusk-bearing, very fine- to fine-grained, bioturbated sandstone (informally called sandstone sequences A, B, C, and D; see correlation diagram, Plate

AI). The sandstone sequences range from 5 ft to 31 ft thick. Sandstone sequences A, B, C, and D are separated by four units of massive, finely micaceous, medium gray siltstone (informally called units 1 through 4 from base to top; Plate AI). In thin sections, the very fine- to fine-grained quartzo-feldspathic-lithic (volcanic) mica-bearing Astoria sandstones are moderately well indurated due to extensive sparry calcite and clay rim cement and some detrital clay. In contrast, the darker gray deeper marine (outer shelf and upper slope?), foram-bearing, micro-micaceous siltstone units are composed of expandable iron-rich smectite clay (see XRD analysis section, Figures A3a, A3b, and A3c) and silt-sized angular quartz, plagioclase feldspar, pyrite, carbonized wood, and mica and are relatively less indurated (less strong). Siltstone unit 2 contains the active basal slip plane (based on inclinometer data) in boreholes LT-1, LT-2, and LT-3, suggesting some stratigraphic control on the landslide (Plate AI).

Sandstone sequences A, B, C, and D and siltstone units 1, 2, and 3 are correlated on a 3.63:1 scale correlation diagram (Plate AI) between the boreholes by stratigraphic position, regional strike and westward dip, similar fossils, internal stratigraphy, distinctive fragments of calcite-replaced pumice in a fine-grained bioturbated sandstone sequence, and adjacent altered glass shard-bearing tuff marker beds. In addition, the yellowish brown, 10- to 11-ft-thick very fine- to fine-grained, shallow-marine, calcite-cemented sandstone D with large fossil scallops (*Patinopecten*) at the base of the sea cliff sections can be traced laterally and mapped (e.g., G. Priest, Figure A2) north-south along the Johnson Creek landslide sea cliff. This sandstone sequence occurs with blocky jointed, thin tuffs at the top and base and an underlying distinctive, thin, buff, concretionary, foram-rich rib-forming bed in the underlying siltstone unit 3 (Plate AI middle sea cliff section). Sandstone sequence D, the underlying *Dentalium*- (tusk

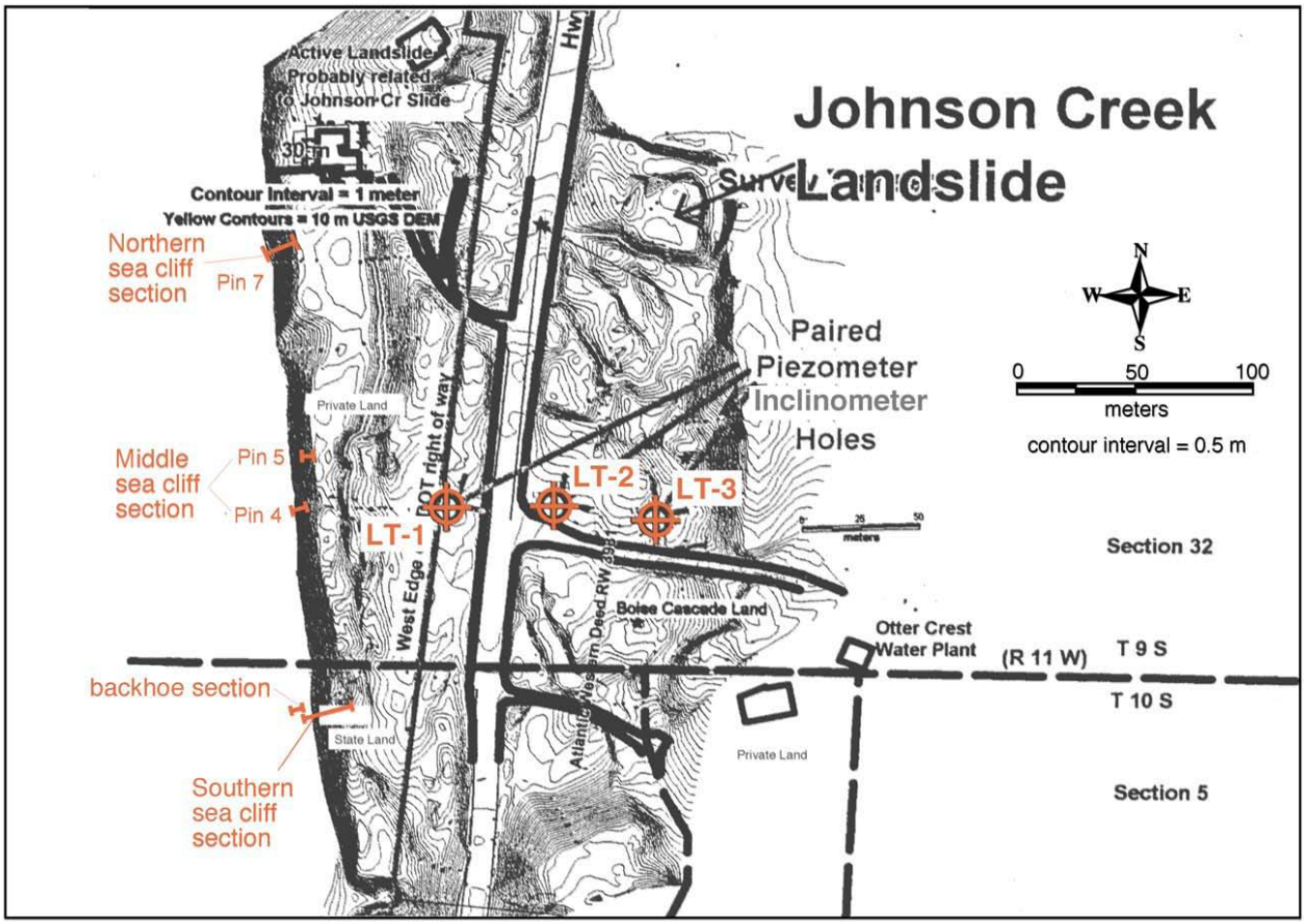

Figure A1. Index map of study area, showing line of cross section (Plate AI).

shell) bearing siltstone unit 3, and the overlying thick massive siltstone (unit 4) with horizons of calcareous concretions overlain by Pleistocene terrace/Holocene sand colluvium are in separate, back-rotated eastward dipping landslide blocks as shown in an east-west cross section (Plate AI). These borehole and outcrop data were used in reconstructing two small east-west cross sections (A and B) of the Johnson Creek translational slide (before sliding, A; and after sliding, B).

In cross section B on Plate AI (no vertical exaggeration), correlation lines connecting Astoria sandstone sequence C and siltstone units 2 and 3 dip 17° westward above the active basal slip plane. Correlated sandstone sequences A and B and siltstone unit 1 (a more confident correlation between boreholes) also dip 17 to 20° west below the active slip plane. The dip of these correlation lines and calculated dips closely match the regional dips measured with a Brunton compass in an Astoria Formation wave-cut bench 150 ft west of the Johnson Creek landslide sea cliff by Alan Niem and just east of the headscarp mapped by George Priest (Figure A2) range from 17° to 20° west. Dips measured on rare bedding in the cores of the three boreholes during drilling (measured by Beckstrand, Niem, and Priest) average 17° but range from 10° to 20° (Plate AI). The lower dip amounts measured below the slip plane could be explained by (a) drag or displacement of different blocks of Astoria Formation by three postulated normal or oblique-slip faults (drawn to make a balanced cross section) or (b) inaccuracy of correlation or drafting or variation (plus or minus a few degrees) of measuring field and core attitudes (i.e., strikes and dips).

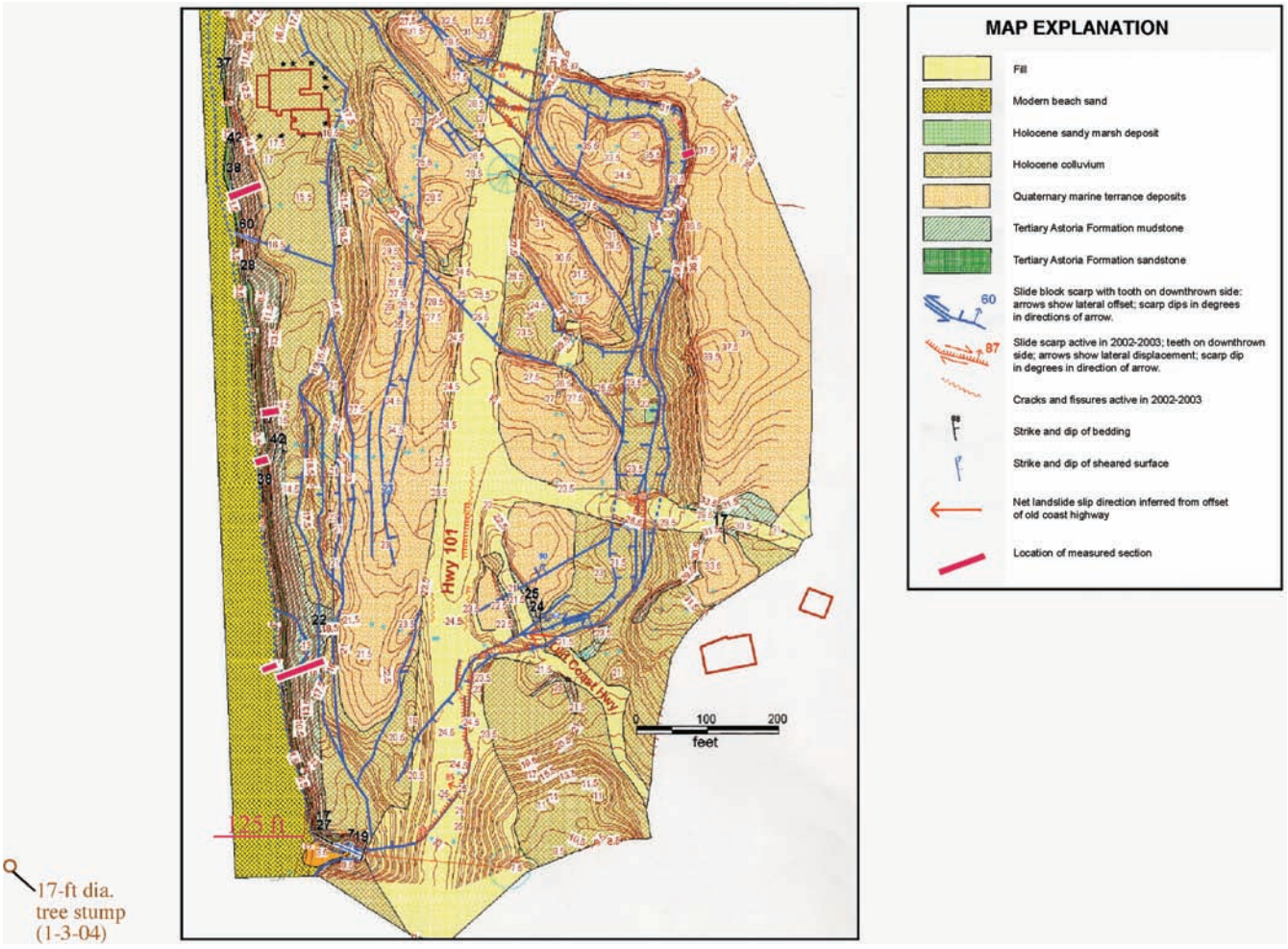

Figure A2. Geologic map of the Johnson Creek landslide study area (from G. Priest; updated January 3, 2004, by A. R. Niem and W. A. Niem).

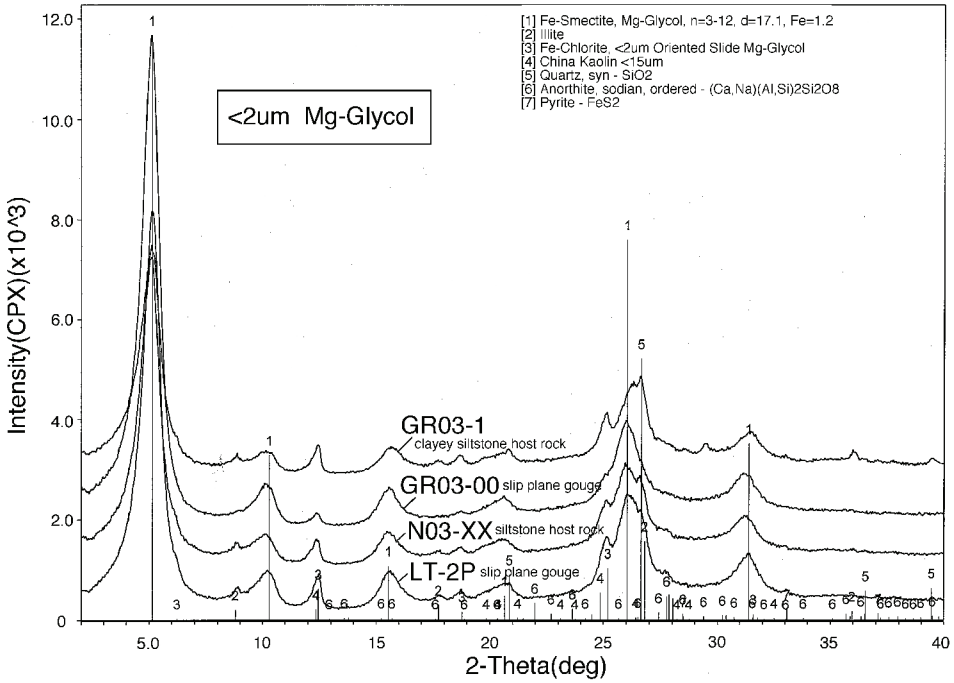

Figure A3a. Comparison of the X-ray diffraction patterns of clay-sized fraction (<2 microns) of four samples: Mg-saturated glycolated host rock in sea cliff (GR03-1), gouge in basal slip plane at the sea cliff (GR03-00, siltstone unit 3), core sample of host rock clayey siltstone (siltstone unit 2) at 54 ft (N03-XX), and clay-silt gouge in basal slip plane at 58.1 ft (borehole LT-2p). All four samples contain mainly expandable Fe-smectite clay matrix (large peak labeled 1) with minor (smaller peaks) detrital illite, Fe-chlorite, possible kaolinite, quartz, anorthite, and diagenetic pyrite. The similarity of peaks suggests the host rock siltstone is the parent rock for the slip plane gouge.

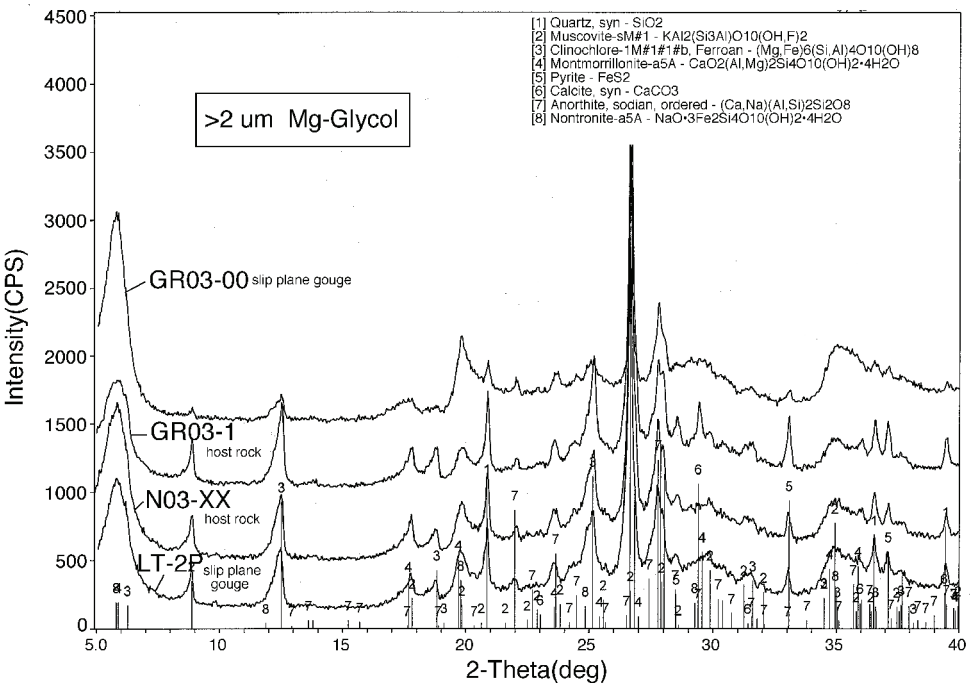

Figure A3b. X-ray diffraction patterns of the silt-sized fraction (>2 microns) of the clay-silt gouge of the basal slip plane show that the gouge contains detrital quartz, calcic plagioclase (i.e., anorthite Na, Ca), pyrite, muscovite, chlorite, nontronite (Fe-smectite), and calcite.

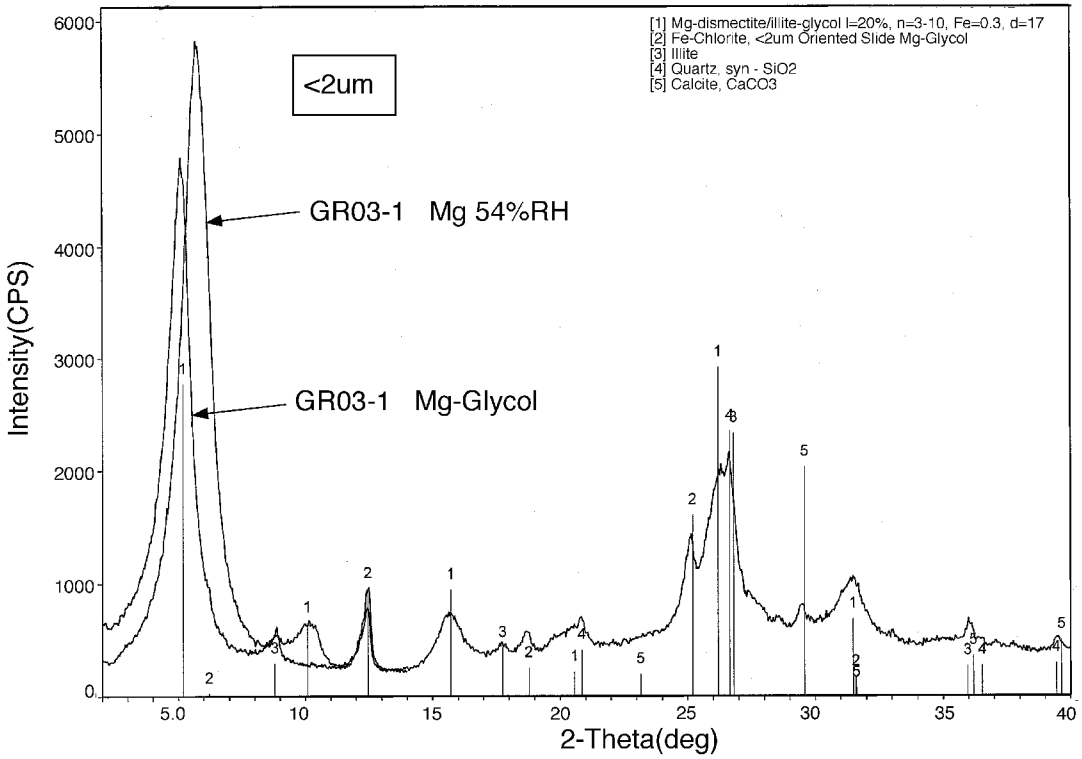

Figure A3c. X-ray diffraction pattern of the clay-sized fraction (<2 microns) of the host rock siltstone (siltstone unit 3) that contains the active slip plane at the base of the sea cliff outcrop. Note the shift to lower 2-theta value of the smectite peak upon glycolation. Other clay-sized components include detrital Fe-chlorite, illite, quartz, and calcite.

2. X-Ray Diffraction Study of the Mineralogical and Microscopic (i.e., SEM) Causes of Slope Failure

The active basal slip plane in the boreholes consists of a thin sheared gouge of wet, soft, medium gray, sheared clayey siltstone. This wet sticky gouge could be easily rolled and molded into long threads between the thumb and index finger, suggesting a moderate clay content. Due to the soft wet nature of the slide plane gouge, recovery was usually poor. A Shelby tube sample of the slide plane gouge (from LT-2P at 59-60 ft) from Landslide Technology underwent XRD analysis but not hydrometer or sieve size analysis. However, a sample of the nearby host clayey siltstone (core sample N03-XX at 54 ft in LT-2) has the same mineralogy (see later XRD discussion) and contains 24.5% clay, 74.6% silt, and 0.9% sand (Table A1).

Based upon inclinometer depths to the basal slip plane and construction of a 1:1 cross section (on Plate AI), the slip plane dips 17° westward between boreholes LT-3 and LT-2 and flattens to 8° westward between LT-

Table A1. Size statistics data.

Sample No.	Percent Sand	Percent Silt	Percent Clay
GR03-00	0.6	93.1	6.3
GR03-1	12.8	74.5	12.7
GR03-5	0.3	79.4	20.3
GR03-6	13	66	21
GR03-7	37.5	55.8	6.7
GR03-8	71	24.6	4.4
GR03-9	5.6	87.7	6.7
GR03-10	5.7	76.9	17.4
GR03-13	31	57	12
N03-32	67.1	32.4	0.5
N03-53	79	20.5	0.5
N03-XX (LT-2 @ 54 ft)	0.9	74.6	24.5
Pin03-2	76	17.5	6.5
Pin03-4a	51.7	32.6	15.7

Shaded cells indicate siltstone samples, including slip plane gouge sample (GR03-00) at base of southern sea cliff section. Other samples are sandstone.

2 and LT-1 (cross section B, Plate AI). The slip plane is just below sea level (NAVD 1983) and then curves up to the surface at the beach, cutting across sandstone sequences C and D and siltstone units 3 and 4 and forming a low bench that is seasonally covered by beach sand. A backhoe excavation of the slip plane near where it emerges on the beach (supervised by George Priest) and winter field observations of the low wave-cut bench that contains the slip plane at the base of the sea cliff suggest the slip plane is nearly horizontal at the surface and then dips 35° eastward thrusted out over 3 to 4.5 ft of modern winter beach heavy mineral sand, sandstone boulder talus, and a basal shelly basalt gravel and underlying intact siltstone unit 4 (bedrock). The basal slip plane gouge, which was temporarily exposed in February 2003 on the wave-cut platform below the southern sea cliff measured section, was sampled (sample GR03-00) and underwent XRD and hydrometer/sieve size analysis. It consists of 6.3 wt % clay size grains, 93.1 wt % silt, and 0.6 wt % sand (Table A1; Figure A4). It was surprising that the wet, plastic (i.e., moderate plasticity) siltstone gouge sample did not have more clay than indicated by the hydrometer grain size analysis because it felt sticky and easily rolled into a ball and thread (see further discussion in section on grain size analysis of siltstones).

Overlying the thin basal slip plane shear gouge (soft, micro-slickensided wet clayey silt) are 10 or more feet of landslide toe breccia, consisting of very poorly sorted, angular broken blocks of *Dentalium*-bearing

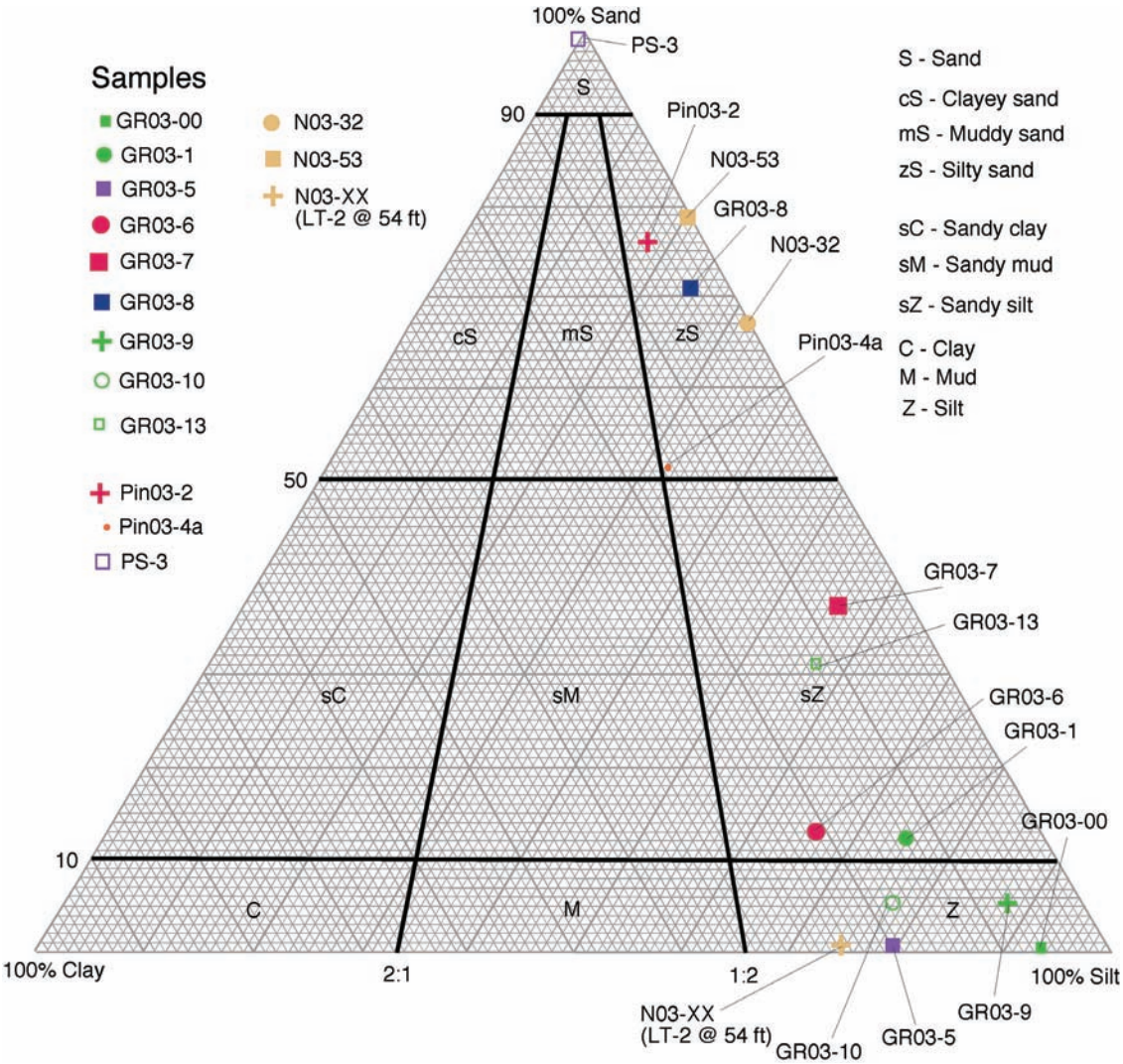

Figure A4. Grain size classification of disaggregated lower and middle Miocene Astoria Formation sandstones and siltstones from sea cliffs at the toe of the Johnson Creek landslide and from cored boreholes LT-1, LT-2, and LT-3. Grain sizes from sieve and hydrometer analysis Triangular classification diagram of sediments by Folk (1974).

siltstone unit 3 (the host rock) in a sheared clayey(?) silt matrix. The breccia is locally overlain by intact (nearly unfractured) siltstone unit 3 that occurs just below sandstone sequence D in the southern sea cliff measured section. The sample of host rock siltstone unit 3 (sample GR03-1) consists of 12.7% clay, 74.5% silt, and 12.89% sand (Table A1). Landslide breccia also appears as a 16-ft-thick section of subhorizontal landslide breccia zones (composed of angular mudstone clasts and chips in clayey silty gouge) and intervening intact siltstone unit 2 in the lower part of borehole LT-1 (Plate AI). The active basal slip plane in LT-1, based upon inclinometer data, lies in the middle of this brecciated zone and includes many overlying and underlying high-angle, slickensided, open (or clay or iron oxide filled) planar extensional fractures that could act as permeable avenues for groundwater flow. Similar extensional high-angle fractures with normal listric slip of a few to several meters occur above the basal slip plane gouge and landslide breccia zone in the sea cliffs at the toe of the landslide (i.e., west end of cross section B).

XRD analysis of the clay mineralogy of the basal slip plane clay-silt gouge in LT-2 (sample LT-2P Shelby tube at 59-60 ft, siltstone unit 2, in Figure A3a) and in the sea cliff outcrop (siltstone unit 3; sample GR03-00) shows that the clay-sized fraction (<2 microns) in this gouge is composed mainly of expandable iron-rich smectite (clay mineral) with minor amounts of detrital illite (muscovite), chlorite (altered biotite?), and perhaps some kaolinite (kaolin) clay minerals (see XRD pattern Figure A3a). Similarly, XRD analysis reveals that the silt-sized fraction (>2 microns) of the gouge contains detrital quartz, calcic plagioclase (i.e., anorthite Na, Ca), pyrite, muscovite, chlorite (clinochlore; altered biotite?), nontronite (Fe-smectite), and calcite (see XRD pattern Figure A3b). X-ray diffraction and thin section study show that these clay mineral types and other minerals are identical to the minerals in samples (e.g., outcrop sample GR03-1 and core sample N03-XX from 54 ft in LT-2) of the adjacent foram-bearing host rock siltstone (units 3 and 2) (see XRD pattern of host rock sample GR03-1 and N03-XX; Figures A3a and A3b). SEM photomicrographs of the sheared gouge show that the expandable iron-rich smectite clay (nontronite?) has been crudely aligned parallel to the slip planes and contains micro-slickensides and sheared and broken foram microfossil tests as a result of this slippage (Figures A5a, A5b, and A5c) suggesting a preferred zone or plane of

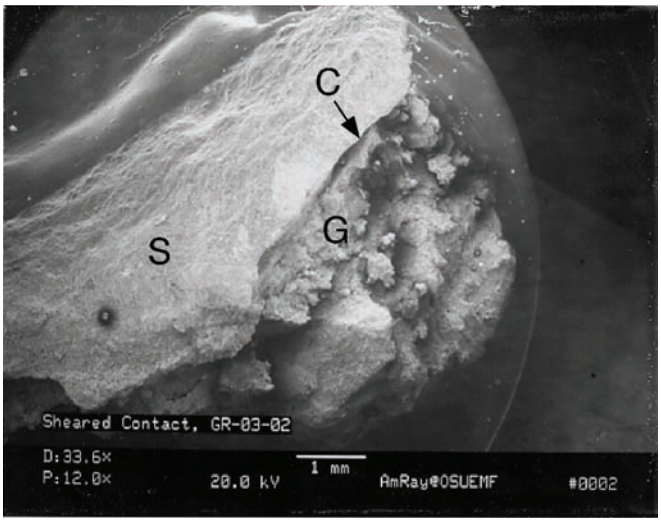

Figure A5a. SEM photomicrograph of sheared contact (sample GR03-02) shows the contact of the undeformed host siltstone (labeled S) with broken fragmented clay-silt gouge (note angular broken siltstone fragments labeled G). The dark crack (labeled C) is the sharp 2-mm-thick contact. Note 1-mm bar scale in bottom margin of photo.

Figure A5b. SEM photomicrograph at low magnification (12.5×) shows a sharp smooth shear plane (labeled Fr) that appears to step across the specimen. The specimen was mounted upside-down, which places the shear gouge (g) in the upper NW half of the photograph and the unsheared siltstone (s) in the lower SE half of the photograph. The sheared gouge appears as a jumbled mass of largely subparallel (imbricated) smectite clay particles or packets. In the gouge, multiple fractures (dark lines), along which slippage has occurred, are subparallel the main shear boundary.

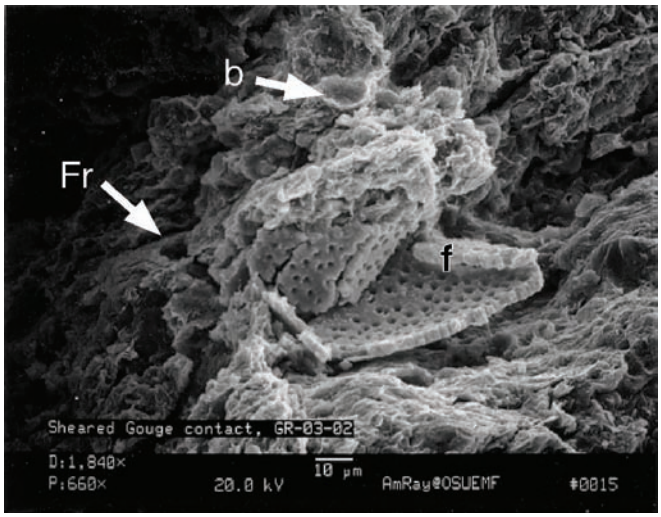

Figure A5c. SEM photomicrograph of bent and broken test (shell) of benthonic foraminer (f) along a fracture (Fr). Flake of biotite (mica) is labeled b.

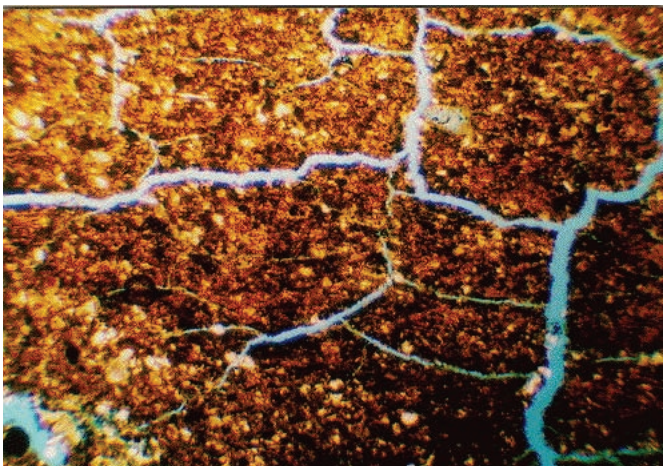

Figure A6. Photomicrograph of dessication microfractures in siltstone sample N03-XX (borehole LT-2 at 54 ft). Microfractures were created as the sample was dried and heated in the process of preparing the thin section. Blue-dyed epoxy fills the microfractures (3.5×, plane-polarized light).

weakness and residual strength. Thin section and SEM photomicrographs also show that many intersecting microdehydration cracks can develop in the expandable smectite-rich gouge as a result of sample preparation (drying and dehydration; Figure A6). It is suggested that these microfractures could also form naturally and could represent avenues for groundwater flow which could further weather the gouge and weaken the cohesion and residual strength by chemical reactions (e.g., dehydration and rehydration of expandable smectite clay in the gouge zone due to seasonal fluctuations of the groundwater table related to rainfall). Groundwater access to such confined microfracture porosity in the slip plane could reduce frictional resistance force and increase the upward normal pressure on the overlying less permeable intact host clayey siltstone in the slide block overlying the basal slip plane.

3. Grain Size Analysis of Sedimentary Units in Johnson Creek Landslide and Their Potential Contribution to the Modern Littoral Budget

Sieve and hydrometer grain size analysis was conducted on 12 Astoria Formation sandstone and siltstone samples (Tables A1 and A2). Most samples are from the southern sea cliff measured section at the toe of the Johnson Creek landslide (i.e., sandstone sequence D and siltstone units 2, 3, and 4), but some came from the borehole cores, including siltstone unit 2 (Figures A1 and A2). Three samples of modern (Holocene) beach and dune sands also were sieved (Table A2). Comparison of the grain size distribution and size statistics of these samples (modern sands and bedrock) allowed preliminary conclusions about how much sand from the Astoria Formation strata in the Johnson Creek sea cliffs contributes to the modern littoral sand budget (task 3 of the contract). The slip plane siltstone gouge and siltstone unit samples[1] plot on a triangular sediment classification diagram (Figure A4) as siltstone or sandy siltstone (% clay ranges from 6.3% to 24.5%, averaging 14.3%), but we believe these rocks may contain more clay and less silt by weight than shown by the hydrometer settling tube analysis, perhaps due to incomplete disaggregation or some flocculation of clay-size grains as silt-sized flocs even though a deflocculating agent (sodium phosphate) was used. Initial visual thin section

1. Civil engineers and engineering geologists generally use the ASTM classification of sediments (e.g., used by ODOT; Bernie Kleutsch, 2003, personal communication) in which mud (i.e., mudstone) includes both silt-sized (siltstone) and clay-sized (claystone) sediment grains for geotechnical purposes. Muds (mudstones) are further differentiated in the Wentworth (1922) and National Research Council classifications used by many geologists. Figure A9 is a comparison of these scales used by engineers and geologists. We prefer to use the term siltstone in this preliminary report to agree with our hydrometer grain size analysis, with the sediment classification of Folk (Figure A4), and with the definition of the Astoria Formation by Snavely and others (1976, 1964) as sandstone, siltstone, and tuff on their regional geologic maps and reports in the Newport area.

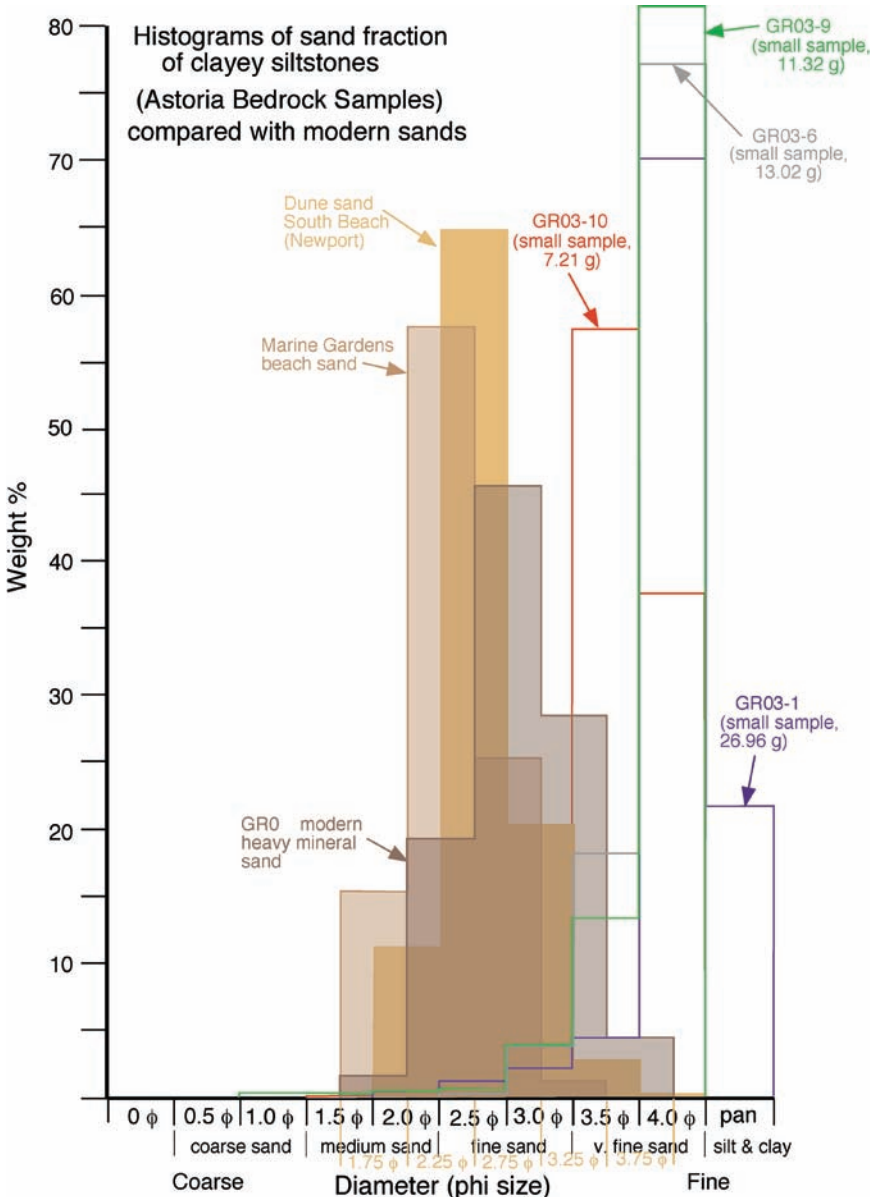

Figure A7. Histograms of sand fraction of Astoria Formation clayey siltstones and siltstones compared with modern sands.

estimates suggest that these rocks should be classified as clayey siltstone or sandy clayey siltstone.

Binocular microscope study and grain size statistics of siltstone units 3 and 4 that comprise the dominant Astoria lithology in the Johnson Creek landslide sea cliffs (Figure A2) suggest the minor sand fraction (<10%) of samples from siltstone units 3 and 4 is too fine-grained (i.e., mainly very fine sand) and partly the wrong mineral composition to contribute much to the coarser grained (i.e., largely fine and some medium sand) modern winter beach sands (Table A2 and Figures A7 and A8). The very fine sand fraction of the Astoria siltstone units, for example, is rich in grains of muscovite, biotite, chlorite, quartz, feldspar, and pyrite. In contrast, the very fine sand size fraction of some modern winter beach sands (e.g., at the base of the Johnson Creek landslide sea cliffs; sample GR0, Table A2) is a largely different mineralogy. The very fine sand-size fraction is composed mainly of dark-colored heavy minerals magnetite/ilmenite, garnet, pyroxene, zircon,

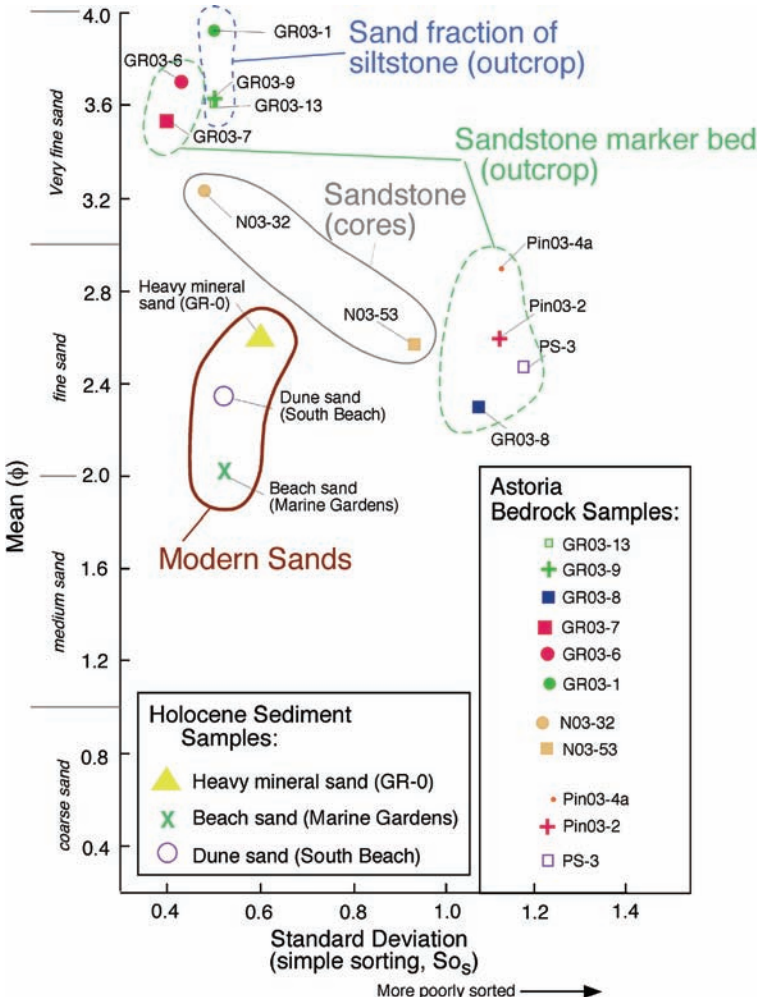

Figure A8. Binary plot of mean size versus standard deviation compares grain sizes of modern beach sands with grain sizes of bedrock. After Friedman (1962).

Comparison of Size Scales *

U.S. Std. Sieve No.	ASTM ODOT	Phi	mm	Wentworth (1922)	National Research Council
		-12	4096	Boulder gravel	VL boulders
		-11	2048		L boulders
	Boulders	-10	1024		M boulders
		-9	512		S boulders
12" (300 mm)		-8	256	Cobble gravel	L cobbles
	Cobbles	-7	128		S cobbles
3" (75 mm)		-6	64	Pebble gravel	VC gravel
	C. gravel	-5	32		C gravel
3/4" (19 mm)		-4	16		M gravel
5/16	F. gravel	-3	8		F gravel
4 5	C sand	-2	4	Granule gravel	VF gravel
10		-1	2	VC sand	VC sand
18	M sand	0	1	C sand	C sand
35 40		1	1/2	M sand	M sand
60	F sand	2	1/4	F sand	F sand
120		3	1/8	VF sand	VF sand
200 230		4	1/16	Silt	C silt
		5	1/32		M silt
		6	1/64		F silt
	Silt and Clay	7	1/128		VF silt
		8	1/256	Clay	C clay-size
		9	1/512		M clay-size
		10	1/1024		F clay-size
		11	1/2048		VF clay-size
		12	1/4096		

* Wentworth and Nat'l. Research Council scales used in this report.

Figure A9. Comparison of grain size scales used by geologists and by engineers.

tourmaline, hypersthene and other heavies and some very fine sand-sized grains of quartz and feldspar.

Some very fine- to fine-grained poorly sorted, bioturbated, shallow-marine Astoria silty sandstones, such as the 10- to 11-ft-thick sandstone sequence D in the lower sea cliff at the toe of the landslide, could contribute 60 to 70% of its weight and volume (visually estimated in thin section) as compositionally similar fine[2] sand-sized grains to the fine sand fraction of the quartz- and feldspar-rich modern beach sand. However, a large proportion (estimated 30 to 40 wt. %) of the sieved Astoria sandstone samples, in statistical plots of mean size, standard deviation (a measure of sorting), and median size, is generally finer grained and more poorly sorted than the modern beach sands (Figures A10, A11, A12, and A13). Modern beach and Astoria sandstone bedrock and core samples generally overlap in skewness (a measure of the asymmetry of the grain size distribution). Quartz and feldspar grains in the Astoria Formation also are more angular than in the modern sand. A modern beach sand sample from near Otter Rock also contains, in addition to fine sand-sized quartz, feldspar, and very fine sand-sized dark-colored heavy minerals, well-rounded very coarse to medium

2. Note: the ASTM engineer's verbal and quantitative limits for sieved sand sizes are slightly different than the geologist's Wentworth (1922) scale and National Research Council scale. In this report, we use the Wentworth's scale, National Research Council scale, and phi scale (see Figure A9 for comparison).

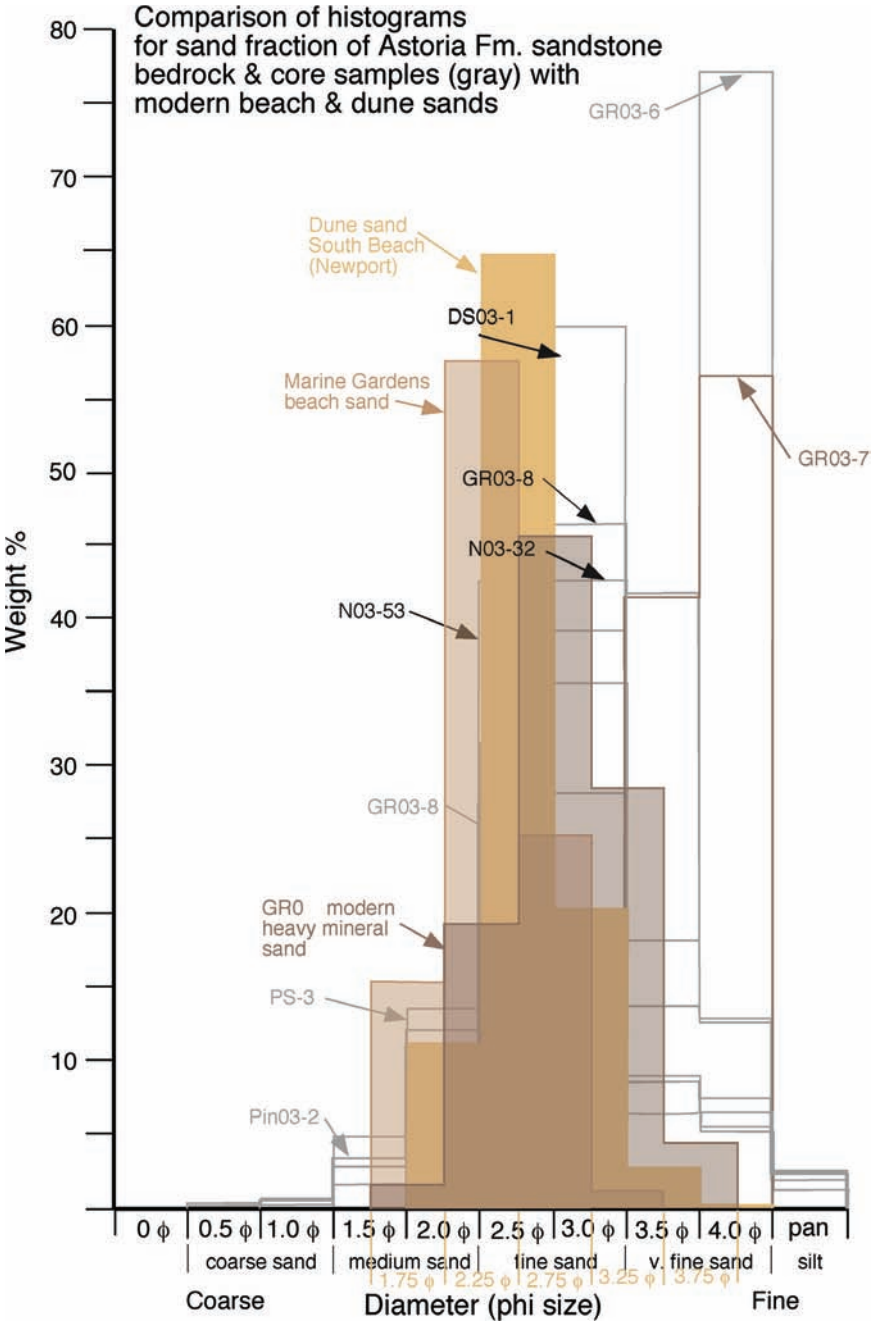

Figure A10. Comparison of histograms for sand fraction of Astoria Formation sandstone bedrock and core samples (gray) with modern beach sands and dune sands. The modern sands are distinctly coarser grained than the sand fraction in the bedrock.

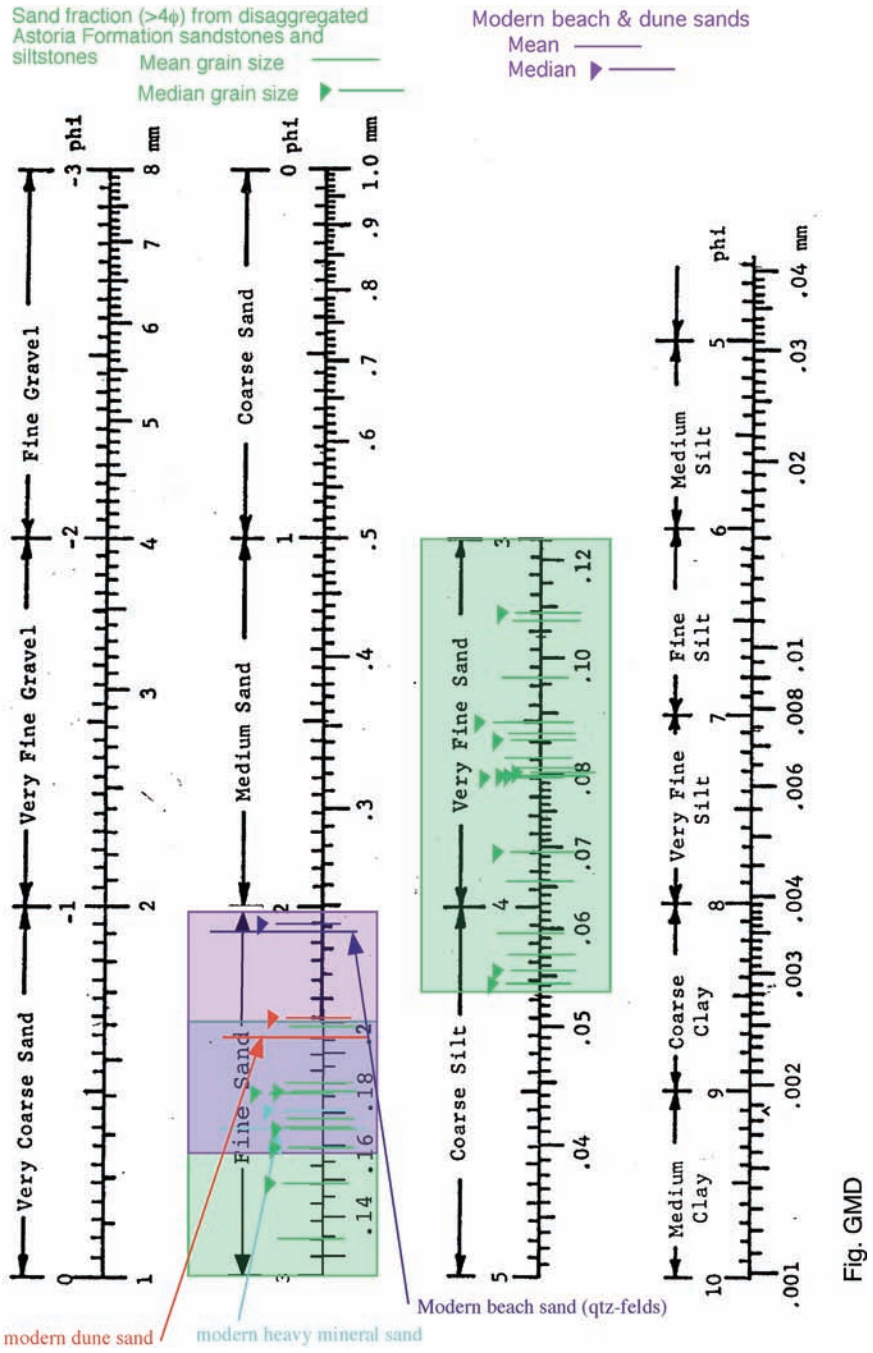

Figure A11. Nomogram with ranges of mean and median grain sizes of Astoria Formation (bedrock) samples and modern beach samples.

sand-sized fragments of middle Miocene Columbia River Basalt derived from nearby basalt headlands and sea stacks (such as Cape Foulweather). This younger basalt unit overlies and invasively intruded (as dikes and sills) the older Astoria Formation. In contrast, the Miocene Astoria strata in thin section contain fine- and some medium sand-sized fragments of andesite/basalt lava derived from the western Cascades volcanic arc and texturally distinct basalt clasts eroded from older Coast Range Eocene basalts, very coarse sand-sized grains of calcite-replaced pumice, metamorphic rock fragments, micas, green hornblende, pyrite, and carbonized wood

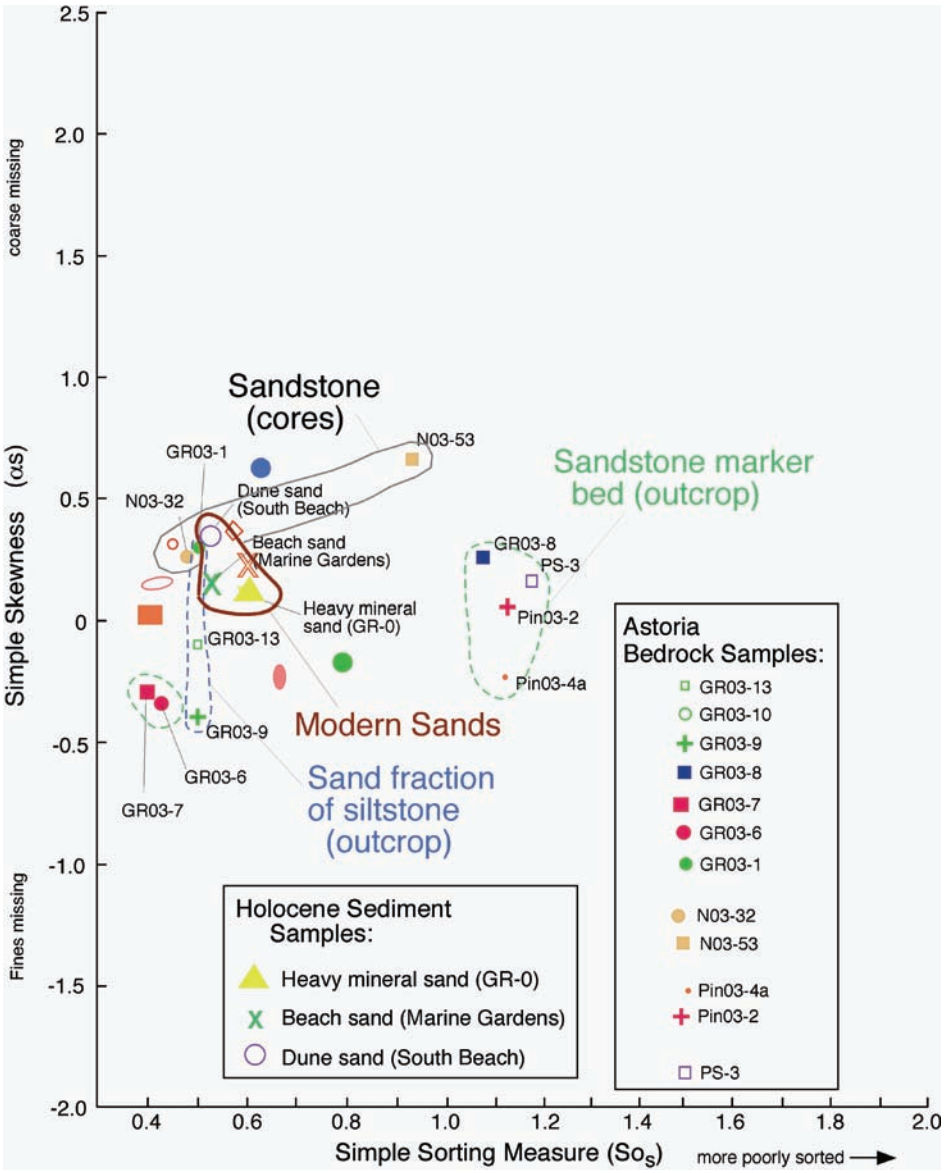

Figure A12. Binary plot of simple skewness versus simple sorting compares sand-sized fraction of Astoria Formation (bedrock) samples with modern sands (beach and dune). After Friedman (1962).

as well as silt-sized quartz and feldspar and clay-sized grains that form a visually estimated 30 to 40% of the total volume. These types of mineral and lithic (rock fragment) grains do not contribute to the modern littoral quartz-feldspar-heavy mineral-rich sand budget because they are either different in composition (Table A2) and/or some of the Astoria quartz and feldspar framework grains are too fine grained (i.e., silt sized to very fine sand sized) to supply grain sizes that comprise the modern, largely fine (and some medium), quartz-feldspar-heavy mineral beach sand (Figure A10). Thus, a large proportion of the 10- to 11-ft-thick sandstone sequence D in the sea cliff at the toe of the landslide probably contributes an estimated only 60 to 70 percent of compositionally similar grain sizes (i.e., quartz, feldspar and heavy minerals) to the modern beach sand. This sandstone sequence also comprises an estimated less than 25% of the total stratigraphic section exposed in the sea cliffs at the toe of the Johnson Creek landslide that includes mainly siltstone units 3 and 4, Pleistocene terrace deposit, and Holocene colluvium (see middle sea cliff section on Plate AI and Figure A2).

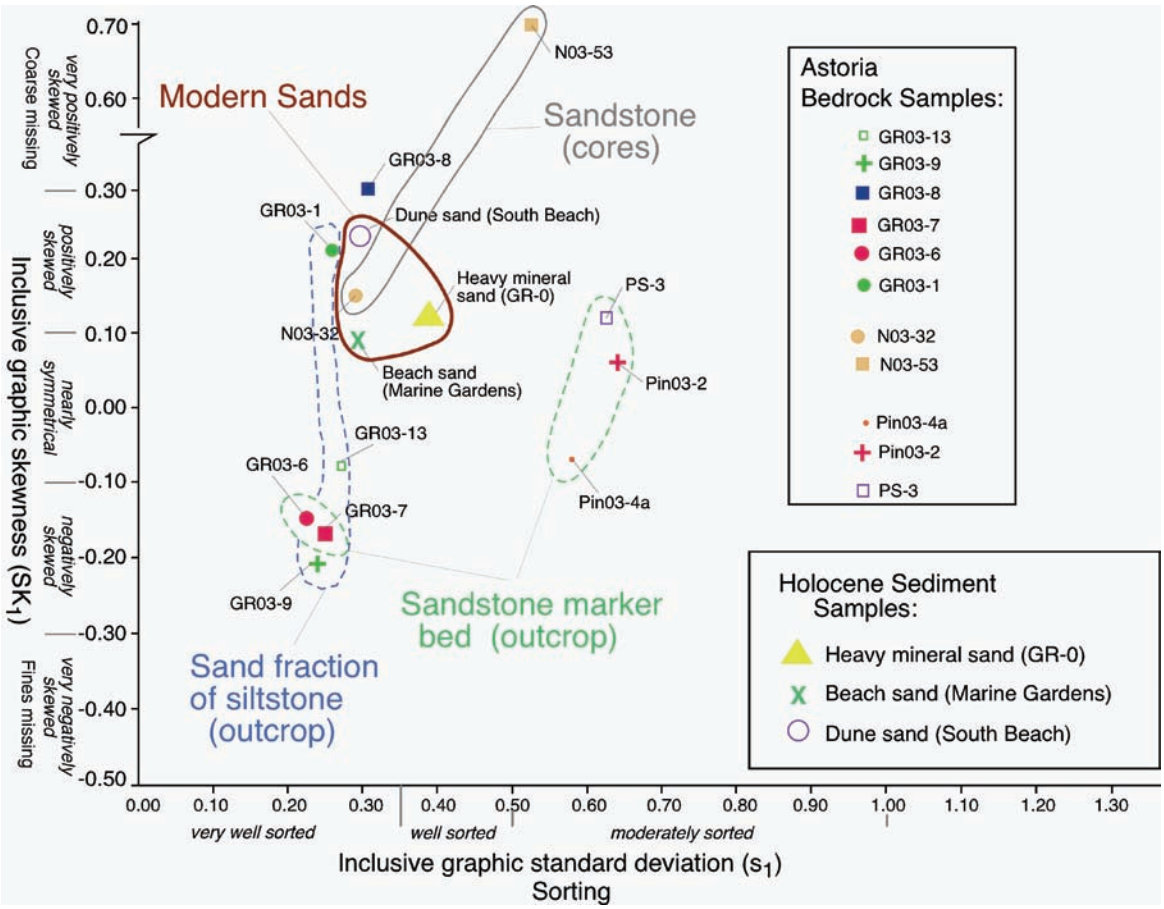

Figure A13. Binary plot of inclusive graphic standard deviation (representing sorting) versus inclusive graphic skewness for sand-sized fraction of Astoria Formation (bedrock) samples compared to modern sand samples (beach and dune). After Friedman (1962).

Ongoing grain size, thin section, and binocular microscope study of some Pleistocene terrace sand samples from the Johnson Creek landslide suggest these friable, fine to medium sands may contribute much more compositionally similar (i.e., rounded quartz and feldspar and similar heavy minerals) grain sizes to the littoral sand budget than the Astoria Formation sandstone and siltstone. However, some fine to coarse beach/fluvial terrace sand and gravels in the Johnson Creek landslide are lithic (rock fragments) -rich (mudstone, volcanics, quartz, agate) and contribute little compositionally to the modern littoral quartz- and feldspar-rich sands. Alternatively, much of the modern fine beach sand (quartz, feldspar, and heavy minerals) could have been recycled from other sources, such as from major rivers like the Umpqua and Columbia during sea level lowstands during Pleistocene glacial stages. These sands were transported northward and southward along an ancient shoreline now on the middle shelf. As sea level rose, eroding and drowning the coastline, the shoreline sand that prograded landward by waves subsequently became trapped with winter beach gravels (basalts) in littoral cells between Miocene basalt headlands. In addition, within the Yaquina Head/Cape Foulweather littoral cell that includes the Johnson Creek landslide, small modern streams (e.g., Wade, Schooner, Johnson, Spencer creeks) have drainage basins headed in older formations (such as the 2000-ft-thick sandstone-rich deltaic Yaquina Formation or widespread older Pleistocene terrace deposits; mapped by Snavely and others, 1976) on older terraced uplands. These small drainage basins could also supply some sand of comparable grain sizes and mineral composition to the modern littoral sand budget.

RECOMMENDATIONS

1. Some additional hydrometer grain size, XRD, thin section, and SEM study of the basal slip plane and Astoria siltstone units in outcrop and core would help define better the mineralogical and micro-textural causes (e.g., percent clay versus silt) of this landslide, which should then be further related to geotechnical engineering properties. A rapid sediment analyzer (sedigraph) could be used to obtain quantitatively more meaningful grain size analysis of percent clay and silt than obtained with a hydrometer. Point counts of percent silt and sand versus clay in thin section would give better quantitative volumetric results than visual estimation.
2. In order to draw a better balanced east-west cross section, a section of the westward-dipping Astoria strata along the Boise Cascade Johnson Creek logging road a short distance east of the headscarp should be measured, described, and projected (i.e., correlate sandstone, tuff and siltstone units) into the east-west correlation diagram to borehole LT-3 (Plate AI, Figures A1 and A2). This east-of-the-headscarp section, unaffected by the Johnson Creek landslide, would help to show the relative movement that has occurred since the slide was initiated. (Time and funds prevent this from being done in this preliminary report.)
3. Additional sieving, pebble counts of gravels, measuring sections at the headscarp and augering the Pleistocene terrace deposit exposed in the headscarp should be conducted to define the geometry of this deposit, the topographic relief on the Pleistocene/Astoria unconformity (e.g., incised paleovalley fill? or wave-cut bench? with surge channels or older landslide or faults). Some additional measured sections along the north-south sea cliff could be measured. Fracture analysis of joints and slip planes in those sections could be done to measure quantitatively the percentage of vertical porosity and permeability. Two north-south geologic cross sections across the Johnson Creek landslide could then be constructed and units correlated to augment the east-west cross section — one section at the headscarp at the eastern end of the Johnson Creek landslide and the other section along the beach sea cliffs. A three-dimensional fence diagram could then be constructed.
4. The contribution of sand-sized sediment from modern streams draining the Astoria and Yaquina formations and Pleistocene terrace and other sea cliff exposures of Astoria sandstones in the Yaquina Head-Cape Foulweather littoral cell should be studied by sieving, thin section (i.e., point counting), and field examination in order to determine the potential of these units to contribute similar size sediment to the littoral sand budget and to calculate the volume of sediment shed from these units. Such studies would provide better quantitative information with the sea cliff erosion studies being conducted by Jon Allan. The Astoria Formation samples from the Johnson Creek landslide study represent only 140 ft of the entire 1,000-ft plus Astoria section; this small sampling may not be representative of the potential grain size contribution of the entire sea cliff section in this cell.

REFERENCES

Folk, R. L., 1974, Petrology of sedimentary rocks: Hemphill, Austin, Tex., 182 p.

Friedman, G. M., 1962, Comparison of moment measures for sieving and thin section data in sedimentary and petrological studies: Journal of Sedimentary Petrology, v. 32, p. 15–25.

Snavely, P. D., Jr., Rau, W. W., and Wagner, H. C., 1964, Miocene stratigraphy of the Yaquina Bay area, Newport, Oregon: The Ore Bin, v. 26, no. 8, p. 133–151.

Snavely, P. D., Jr., MacLeod, N. S., Wagner, H. C., and Rau, W. W., 1976, Geologic map of the Cape Foulweather and Euchre Mountain quadrangles, Lincoln County, Oregon: U.S. Geological Survey Misc. Inv. Series Map I-868, scale 1:62,500.

Wentworth, C. K., 1922, A scale of grade and class terms for clastic sediments: Journal of Geology, v. 30, p. 377–392.

Table A2. Percentage sand, silt, and clay in samples.

Easting	Northing	Elevation (m) relative to NAVD 1983	Sample No. *	Location Description	Lithology or Sediment Classification	Principal Minerals	Sample Wt. (g)	Mean (numerical) (φ)	Mean (verbal)	Median (numerical) (φ)	Median (verbal)	Standard Deviation (s1) (φ)	Simple Sorting (numerical) (φ)	Sorting (verbal)	Skewness (numerical) (Sk1) ** (φ)	Skewness (verbal)	Simple skewness (alpha s)	Kurtosis (numerical)	Kurtosis (verbal) ***
2,218,352.78	125,494.11	5.55	Pin03-4a	northern sea cliff section	friable fine to medium grained sandstone	quartz (70–80%), feldspar (5–10%), mica (muscovite) (<3%), heavy minerals (green pyroxenes and opaques) (<6%)	110.09	2.9	fine sand	2.75	fine sand	0.5784	1.13	moderately sorted	-0.07	nearly symmetrical	-0.25	1.84	very leptokurtic
2,218.367.4	125,277.24	2.35	GR03-00	southern sea cliff section	basal gouge	quartz, white and black micas, forams, quartz, translucent heavy minerals	2.74	4.18	coarse silt	4.21	coarse silt	0.3773	0.75	well sorted	-0.55	very negatively skewed		1.81	very leptokurtic
2,218.367.4	125,277.24	3.1	GR03-1	southern sea cliff section	*Dentalium* (fossil scaphopod) -bearing clayey siltstone at base of section	quartz (50%), feldspar (15%), biotite/chlorite (20%), muscovite (10%), opaque heavy minerals (5%), forams (5%)	26.96 (without forams and shell fragments)	3.93	very fine sand	3.85	very fine sand	0.264	0.5	very well sorted	0.21	positively skewed	0.3	4.1	extremely leptokurtic
2,218.367.4	125,277.24	3.7	GR03-5	southern sea cliff section	tuffaceous claystone	quartz, white and black micas, feldspar	1	4.07	coarse silt	4.17	coarse silt	0.3442	0.58	very well sorted	-0.37	very negatively skewed		1.57	very leptokurtic
2,218.367.4	125,277.24	3.85	GR03-6	southern sea cliff section	fine-grained calcite-cemented sandstone		13.02	3.65	very fine sand	3.65	very fine sand	0.2288	0.43	very well sorted	-0.15	slightly negatively skewed	–0.35	1.39	leptokurtic
2,218.367.4	125,277.24	4.6	GR03-7	southern sea cliff section	*Patinopecten* sandstone	quartz (50%) feldspar (40%), white mica + biotite/ chlorite (<2%), translucent heavy minerals (<2%), opaque heavy minerals (ilmenite/magnetite) (<3%), carbonized wood (3%)	57.3	3.53	very fine sand	3.6	very fine sand	0.2462	0.4	very well sorted	-0.17	slightly negatively skewed	–0.3	1.09	mesokurtic
2,218.367.4	125,277.24	5.25	GR03-8	southern sea cliff section	shallow marine fine-grained sandstone	quartz (70%), lithics (24%), feldspars (5%)	128.03	2.3	fine sand	2.65	fine sand	0.3133	1.075	very well sorted	0.3	positively skewed	0.25	1.47	leptokurtic
2,218.367.4	125,277.24	6.75	GR03-9	southern sea cliff section	clayey sandy siltstone - 8″ above 10-11 ft yellow sandstone marker bed	quartz (60%), feldspar (10–15%), biotite (5%), white mica (15%), opaque heavy minerals (5%)	11.32	3.63	very fine sand	3.65	very fine sand	0.239	0.5	very well sorted	-0.21	negatively skewed	–0.4	2.05	very leptokurtic
2,218.367.4	125,277.24	8.28	GR03-10	southern sea cliff section	clayey sandy siltstone 3 to 5 ft below top of sea cliff	quartz (50%), feldspar (20%), mica (10%), opaques (5%), shell fragments (<3%)	7.21	3.5	very fine sand	3.5	very fine sand	0.2538	0.43	very well sorted	-0.06	nearly symmetrical		1.16	leptokurtic

(table continued on next page)

* All samples for size analysis, thin section, SEM, and XRD from the middle and northern sea cliff sections were rock fall collected on the public beach (sand) and correlated to the adjacent sea cliff sections. These sections were measured from the public beach by visually estimating thickness of units using a 3-m pole tilted perpendicular to the angle of dip of the strata in the sea cliff.

Samples from the southern sea cliff section, which was described and measured with a Jacobs staff and Abney level, were collected directly from the coastal sea cliff which is on State of Oregon land.

** Positive skewness = coarse fraction missing. Negative skewness = fine fraction missing.

*** Leptokurtic = very tall peak. Mesokurtic = close to normal curve. Platykurtic = flat curve

Table A2. continued.

Easting	Northing	Elevation (m) relative to NAVD 1983	Sample No. *	Location Description	Lithology or Sediment Classification	Principal Minerals	Sample Wt. (g)	Mean (numerical) (φ)	Mean (verbal)	Median (numerical) (φ)	Median (verbal)	Standard Deviation (s1) (φ)	Simple Sorting (numerical) (φ)	Sorting (verbal)	Skewness (numerical) (Sk1) ** (φ)	Skewness (verbal)	Simple skewness (alpha s)	Kurtosis (numerical)	Kurtosis (verbal) ***
2,218,367.4	125,277.24	14.83	GR03-13	southern sea cliff section	weathered clayey sandy siltstone at 8 ft below top of section	quartz (60%), feldspar (30%), micas (5%), opaque heavy minerals (3%), translucent heavy minerals (2%)	41.65	3.6	very fine sand	3.65	very fine sand	0.264	0.5	very well sorted	-0.08	nearly symmetrical	–0.1	1.37	leptokurtic
2,218,430.39	125,383.68	3.7	N03-32	LT-3 @ 68.4 ft	pumice-bearing fine- to medium-grained fossiliferous sandstone		54.53	3.23	very fine sand	3.2	very fine sand	0.2939	0.48	very well sorted	0.15	slightly positively skewed	0.25	0.87	platykurtic
2,218,515.77	125,374.33	6.3	N03-53	LT-1 @ 58.8 ft	medium-grained sandstone	quartz (75%), lithics (25%)	92.78	2.57	fine sand	2.5	fine sand	0.5303	0.93	moderately sorted	0.7	very positively skewed	0.65	1.26	leptokurtic
2,218,480.36	125,383.12	8.1	N03-XX	LT-2 @ 54 ft	clayey siltstone	quartz, feldspar, white mica, black mica, pyrite, forams	2.94	3.38	very fine sand	3.64	very fine sand	0.6563	1.09	moderately sorted	-1.38	very negatively skewed		0.95	mesokurtic
2,218,352.78	125,494.11	4.35	Pin03-2	northern sea cliff section	calcite-cemented fine- to medium-grained silty sandstone	quartz (70%), feldspar (20%), green translucent lithic (5%), opaque heavy minerals (2%), mica (<1%)	103.6	2.6	fine sand	2.6	fine sand	0.6409	1.125	moderately sorted	0.06	nearly symmetrical	0.05	1.42	leptokurtic
2,218,357.08	125,392.03	4.86	PS-3	middle sea cliff section	calcite-cemented fine- to medium-grained sandstone	quartz (70%), lithics (30%)	195.88	2.47	fine sand	2.5	fine sand	0.63	1.175	moderately sorted	0.12	slightly positively skewed	0.15	1.48	leptokurtic
		6(?)	Holocene dune	South Beach State Park (Newport)	dune sand	quartz (55%), feldspar (30%), translucent heavy minerals (pyroxene, garnet, hornblende, and others) (8%), opaque heavy minerals (7%)	202.48	2.35	fine sand	2.3	fine sand	0.2966	0.525	very well sorted	0.23	positively skewed	0.35	1.43	leptokurtic
		2(?)	Marine Gardens beach sand	Marine Gardens, Otter Rock	winter beach sand		173.11	2.07	fine sand	2.05	fine sand	0.2966	0.525	very well sorted	0.09	nearly symmetrical	0.15	1.08	mesokurtic
2,218,364	125,277	2.2	GR0 heavy mineral beach sand	modern beach, southern sea cliff section	winter beach sand		181.6	2.6	fine sand	2.55	fine sand	0.3943	0.6	well sorted	0.12	positively skewed	0.1	0.89	platykurtic

* All samples for size analysis, thin section, SEM, and XRD from the middle and northern sea cliff sections were rock fall collected on the public beach (sand) and correlated to the adjacent sea cliff sections. These sections were measured from the public beach by visually estimating thickness of units using a 3-m pole tilted perpendicular to the angle of dip of the strata in the sea cliff.

Samples from the southern sea cliff section, which was described and measured with a Jacobs staff and Abney level, were collected directly from the coastal sea cliff which is on State of Oregon land.

** Positive skewness = coarse fraction missing. Negative skewness = fine fraction missing.

*** Leptokurtic = very tall peak. Mesokurtic = close to normal curve. Platykurtic = flat curve.

Oregon Department of Geology and Mineral Industries Special Paper 40
Johnson Creek Landslide Research Project, Lincoln County, Oregon: Final Report
by G. R. Priest, J. C. Allan, A. R. Niem, W. A. Niem, and S. E. Dickenson
Appendix A

Plate I

Preliminary Lithologic Corelation of Boreholes LT-1, LT-2, and LT-3 with outcrop at west toe of Johnson Creek landslide

by A. R. Niem and W. A. Niem

April, 2003

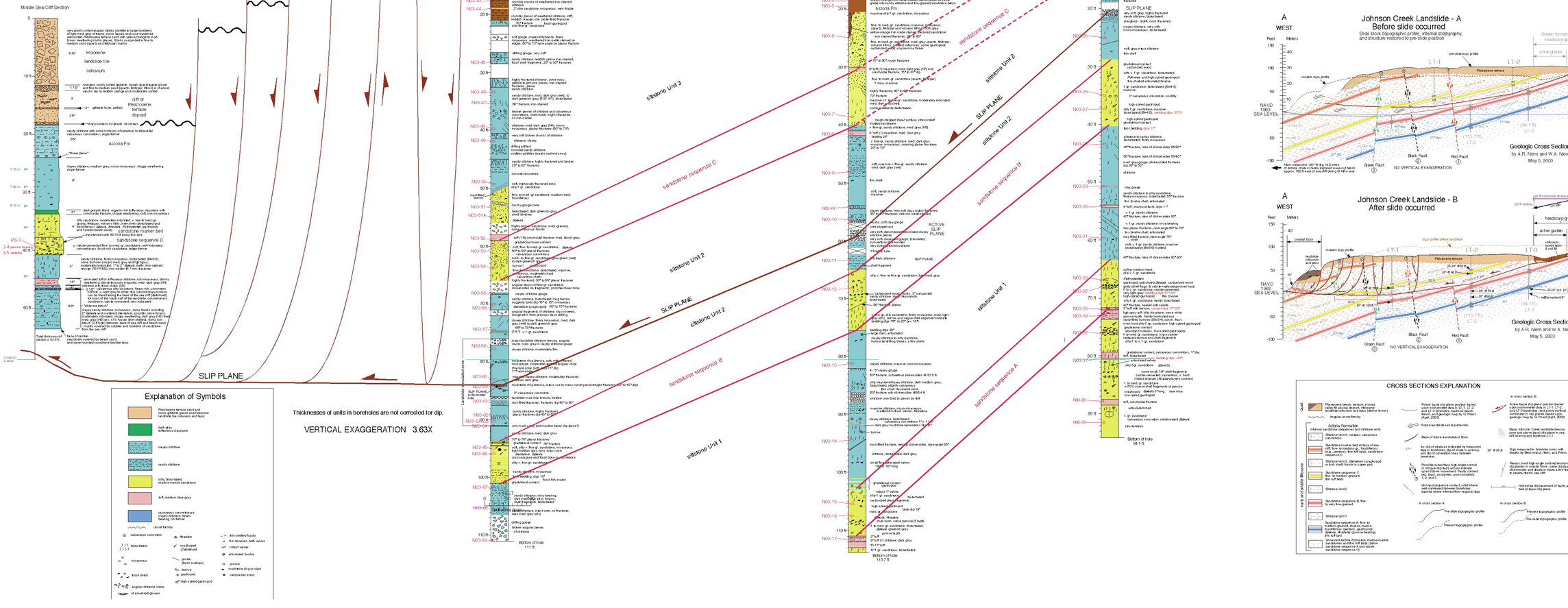

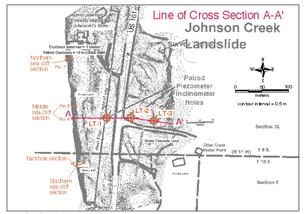

Fig. 1 Line of geologic cross section.